Technical Note - Decoupling the effects of clear atmosphere and clouds to simplify calculations of the broadband solar irradiance at ground level

A. Oumbe[1*], Z. Qu[1], P. Blanc[1], M. Lefèvre[1], L. Wald[1] and S. Cros[2]

[1]{MINES ParisTech, PSL Research University, O.I.E. - Centre Observation, Impacts, Energy - Sophia Antipolis, France}

[2]{Laboratoire de Météorologie Dynamique, IPSL/CNRS, UMR 8539, Ecole Polytechnique, France, now at Reuniwatt, Sainte-Clotilde, Reunion Island, France}

[*]{now at Total New Energies, R&D –Solar, France}

Correspondence to: L. Wald (lucien.wald@mines-paristech.fr)

Abstract

In the case of infinite plane-parallel single- and double-layered cloud, the solar irradiance at ground level computed by a radiative transfer model can be approximated by the product of the irradiance under clear atmosphere and a modification factor due to cloud properties and ground albedo only. Changes in clear-atmosphere properties have negligible effect on the latter so that both terms can be calculated independently. The error made in using this approximation depends mostly on the solar zenith angle, the ground albedo and the cloud optical depth. In most cases, the maximum errors (percentile 95%) on global and direct surface irradiances are less than 15 W m^{-2} and less than 2-5% in relative value. These values are similar to those recommended by the World Meteorological Organization for high quality measurements of the solar irradiance. Practically, the results mean that a model for fast calculation of surface solar irradiance may be separated into two distinct and independent models, possibly abaci-based, whose input parameters and resolutions can be different, and whose creation requires less computation time and resources than a single model.

1 Introduction

Solar radiation drives weather and climate and takes part in the control of atmospheric chemistry. The surface solar irradiance (SSI) is defined as the power received from the sun on a horizontal surface at ground level. Under concern here is the SSI integrated over the whole spectrum, i.e. between 0.3 μm and 4 μm, called total or broadband SSI.

Numerical radiative transfer models (RTM) simulate the propagation of radiation through the atmosphere and are used to calculate the SSI for given atmospheric and surface conditions. RTMs are demanding regarding computer time and in this respect are not appropriate in cases where operational computations of the SSI are performed such as at the Deutscher WetterDienst (Mueller et al., 2009), the Royal Netherlands Meteorological Institute (KNMI) (Deneke, Feijt, and Roebeling, 2008; Greuell, Meirink, and Wang, 2013), the MINES ParisTech (Blanc et al., 2011) or prepared within the MACC European project (Granier et al., 2010). Several solutions have been proposed in order to speed up calculations of the SSI, such as abaci –also known as look-up tables (LUT)– (Deneke, Feijt, and Roebeling, 2008; Huang et al., 2011; Mueller et al., 2009; Schulz et al., 2009).

The present work contributes to the research of fast calculations of the SSI under all sky conditions. It does not propose a new model but an approximation that can be adopted by models for calculations of the SSI. More precisely, it examines whether in the case of infinite plane-parallel single- and double-layered cloud, the SSI computed by a RTM can be approximated by the product of the SSI under clear-sky and a modification factor due to cloud properties and ground albedo only. If this approximation is accurate enough, i.e. if the modification factor does not significantly change with clear-atmosphere properties, it would be possible to construct two independent models, possibly LUT-based models –for example, one for clear-sky conditions, and the other for cloudy conditions. Recently, for example, Huang et al. (2011) used such an approximation with a very limited justification. This Technical Note aims at holding this justification by (1) exploring the influence of the properties of the clear atmosphere on the SSI in cloudy atmosphere, (2) proposing a general equation that decouples the effects of the clear atmosphere from those due to the clouds, and (3) computing the errors made with this approximation.

2 Objective

Let G denote the SSI for any sky. G is the sum of the beam component B of the SSI –also known as the direct component– and of the diffuse component D, both received on a horizontal surface. In the present article, following the RTM way of doing, B does not comprise the circumsolar radiation. Let note G_c, B_c and D_c the same quantities but for clear-sky. The ratios K_c and K_{cb} are called clear-sky indices (Beyer, Costanzo, and Heinemann, 1996):

$$K_c = G / G_c \quad (1)$$

$$K_{cb} = B / B_c$$

K_c is also called cloud modification factor in studies on UV or photosynthetically active radiation (Calbo, Pages, and Gonzalez, 2005; den Outer et al., 2010).

The indices K_c and K_{cb} concentrate the cloud influence on the downwelling radiation and are expected to change with clear-atmosphere properties P_c since the clouds and other atmospheric constituents are mixed up in the atmosphere. Eq. 1 can be expanded:

$$G = G_c(\theta_S, \rho_g, P_c)\, K_c(\theta_S, \rho_g, P_c, P_{cloud}) \quad (2)$$

$$B = B_c(\theta_S, P_c)\, K_{cb}(\theta_S, P_c, P_{cloud})$$

where

- θ_S is the solar zenith angle,
- ρ_g the ground albedo,
- P_c is a set of 7 variables governing the optical state of the atmosphere in clear-sky: *i)* total column contents in ozone and *ii)* water vapour, *iii)* elevation of the ground above mean sea level, *iv)* vertical profile of temperature, pressure, density, and volume mixing ratio for gases as a function of altitude, *v)* aerosol optical depth at 550 nm, *vi)* Angström coefficient, and *vii)* aerosol type,
- P_{cloud} is a set of variables governing the optical state of the cloudy atmosphere: *i)* cloud optical depth (τ_c), *ii)* cloud phase, *iii)* cloud liquid water content, *iv)* droplet effective radius, and *v)* the vertical position of the cloud.

The objective of this article is to quantify the error made in decoupling the effects of the clear atmosphere from those due to the clouds in cloudy sky, i.e. if changes in P_c are neglected in K_c, respectively K_{cb} in Eq. 2. This is equivalent to say that the first derivative $\partial K_c / \partial P_c$, resp. $\partial K_{cb} / \partial P_c$, is close to 0. In that case, Eq. 2 may be replaced by the following approximation:

$$G \approx G_c(\theta_S, \rho_g, P_c)\, K_c(\theta_S, \rho_g, P_{c0}, P_{cloud}) \quad (3)$$

$$B \approx B_c(\theta_S, P_c)\, K_{cb}(\theta_S, P_{c0}, P_{cloud})$$

where P_{c0} is an arbitrarily chosen but typical set P_c. The objective is now to quantify the error made when using Eq. 3 instead of Eq. 2.

3 Method

The methodology used for assessing Eq. 3 is of statistical nature. For a given condition related to the position of the sun, the ground albedo and the clouds (θ_S, ρ_g, P_{cloud}), several sets of clear-sky properties P_c are randomly built. Each 4-tuple (θ_S, ρ_g, P_{cloud}, P_c) is input to a RTM to compute G, B, D, K_c and K_{cb}. The variances of the K_c and K_{cb} series are then computed. The lower the variance, the lower the changes in K_c or K_{cb} with respect to the changes in P_c and the more accurate the approximation given by the Eq. 3. The errors made on the retrieved G and B when using Eq. 3 are quantified.

The RTM libRadtran version 1.7 (Mayer, Kylling, 2005) is used with the DISORT (discrete ordinate technique) algorithm (Stamnes et al. 1988) to solve the radiative transfer equation. libRadtran needs input data of the atmosphere and surface properties. When not provided, data are replaced by standard assumptions. Atmosphere and clouds are assumed to be infinite plane-parallel.

Table 1 reports the range of the ten values taken respectively by θ_S and ρ_g. For computational reasons, θ_S is set to 0.01°, respectively 89° in place of 0°, resp. 90°.

Table 1. Range of values taken by θ_S and ρ_g.

Variable	Range of values
Solar zenithal angle (θ_S)	0.01, 10, 20, 30, 40, 50, 60, 70, 80, 89, in degree
Ground albedo ρ_g	0, 0.05, 0.1, 0.15, 0.2, 0.3, 0.4, 0.5, 0.7, 0.9

Cloud properties input to libRadtran are τ_c, phase –water or ice clouds–, heights of the base and top of cloud, the cloud liquid content and effective radius of the droplets. Default values in libRadtran for cloud liquid content and droplet effective radius are used: 1.0 g m^{-3} and 10 µm for water cloud, and 0.005 g m^{-3} and 20 µm for ice cloud. In a preliminary study (Oumbe, 2009, Fig. 4.6, p. 53), the influence of the changes in effective radius, from 3 to 50 µm was found negligible for ice clouds. For water clouds, the smaller the radius, the greater the influence, though this influence is still negligible with respect to other variables.

The cloud properties are linked together. Table 2 presents the typical height of the base of cloud, geometrical thickness, and τ_c for the different cloud types and is established after Liou (1976), Rossow and Schiffer (1999).

Table 2. Properties of cloud types. Base height and thickness are from Liou (1976), and cloud optical depth are from Rossow and Schiffer (1999). Cu: cumulus, Sc: stratocumulus, As: altostratus, Ac: altocumulus, Ci: cirrus, Cs: cirrostratus.

Cloud type	Base height (km)	Thickness (km)	Cloud optical depth
Low cloud (Cu, Sc)	1.7	0.45	Cu: 0 – 3.6 Sc: 3.6 - 23
Middle cloud (As, Ac)	4.2	0.6	Ac: 0 – 3.6 As: 3.6 - 23
High cloud (Ci, Cs)	4.6	1.7	Ci: 0 – 3.6 Cs: 3.6 - 23
Stratus (St)	1.4	0.1	23 - 379
Nimbostratus (Ns)	1.4	4	23 - 379
Cumulonimbus (Cb)	1.7	6	23 - 379

Ten values of τ_c are selected in this study for water clouds, and ten others for ice clouds (Table 3, left column). Ranges of τ_c are related to types of clouds to reproduce realistic

conditions. Each τ_c defines a series of 7 couples cloud base height-thickness for water clouds and 3 for ice clouds (Table 3).

Table 3. Selected cloud properties

Cloud optical depth	Water cloud (cloud base height + thickness, km)	Ice cloud (cloud base height + thickness, km)
0.5, 1, 2, 3 (and 4 for ice cloud only)	Cu: 0.4+0.2, 1+1.6, 1.2+0.2, 2+0.5 Ac: 2+3, 3.5+1.5, 4.5+1	Ci: 6+0.5, 8+0.3, 10+1
5, 7, 10, 20 (and 15 for ice cloud only)	Sc: 0.5+0.5, 1.5+0.6, 2+1, 2.5+2 As: 2+3, 3.5+2, 4.5+1	Cs: 6+0.5, 8+2, 10+1
40, 70	St: 0.2+0.5, 0.5+0.3, 1+0.5 Ns: 0.8+3, 1+1 Cb: 1+6, 2+8	-

According to Tselioudis, Rossow, and Rind (1992), 58% of the clouds are single-layered and 28% are double-layered. The results presented hereafter are for single-layer; the case of double-layered clouds is briefly discussed at the end of Section 4 as results are similar in both cases.

For a given cloud phase, there are 1000 (10x10x10) possible combinations of θ_S, ρ_g (Table 1) and τ_c (Table 3). The selection of a given τ_c leads to the additional selection of a series of cloud base heights and thicknesses as shown in Table 3, i.e. 7 for water clouds and 3 for ice clouds. At that stage, there are 7000 triplets (θ_S, ρ_g, P_{cloud}) for water clouds and 3000 for ice clouds.

Each triplet (θ_S, ρ_g, P_{cloud}) gives birth to 20 4-tuples (θ_S, ρ_g, P_{cloud}, P_c) by adding 20 P_c randomly selected in Table 4. Similarly to what was done by Lefevre et al. (2013) and Oumbe et al. (2011), the selection takes into account the modelled marginal distribution established from observation. More precisely, the uniform distribution is chosen as a model for marginal probability for all parameters except aerosol optical thickness, Angstrom coefficient, and total column ozone. The chi-square law for aerosol optical thickness, the normal law for the Angstrom coefficient, and the beta law for total column ozone have been selected. The selection of these parametric probability density functions and their corresponding parameters have been empirically determined from the analyses of the observations made in the AERONET network for aerosol properties and from meteorological satellite-based ozone

products (cf. Table 4). For the sake of avoiding non-realistic cases, the allocation of the aerosol types is empirically linked to the ground albedo (Table 5).

Table 4. Range of P_c values (7 variables describing the clear atmosphere).

Variable	Range of values
Total column content in ozone	Ozone content is: 300*β + 200, in Dobson unit. Beta law, with A parameter = 2, and B parameter = 2, to compute β
Total column content in water vapour	Uniform between 0 - 70, in kg/m^2
Elevation of the ground above mean sea level	Equiprobable in the set: 0, 1, 2, 3 in km
Atmospheric profiles (Air Force Geophysics Laboratory standards)	Equiprobable in the set: Midlatitude Summer, Midlatitude Winter, Subarctic Summer, Subarctic Winter, Tropical, U.S. Standard
Aerosol optical depth at 550 nm	Gamma law, with shape parameter = 2, and scale parameter = 0.13
Angstrom coefficient	Normal law, with mean = 1.3 and standard-deviation = 0.5
Aerosol type	Equiprobable in the set of 10 aerosol types proposed in libRadtran: urban, continental average, continental clean, continental polluted, maritime clean, maritime polluted, maritime tropical, desert, antarctic

Table 5. Empirical allocation of aerosol types according to ground albedo

Ground albedo	Possible aerosol types
< 0.1	maritime clean, maritime polluted, maritime tropical
0.1 – 0.2	continental average, continental clean, continental polluted, urban
0.2 – 0.25	continental average, continental clean, continental polluted, urban, desert
0.25 – 0.4	continental average, continental clean, desert
0.4 – 0.5	continental average, continental clean
0.5 – 0.9	continental average, continental clean, antarctic

Each combination (θ_S, ρ_g, P_{cloud}, P_c) is input to libRadtran, yielding G, B, D. In addition, G_c and B_c are obtained by libRadtran using (θ_S, ρ_g, P_c) as inputs. K_c and K_{cb} are obtained using Eq. 1. A series of 140 000 values for G, B, D, K_c and K_{cb} is thus obtained for water clouds and 60 000 for ice clouds. For each triplet (θ_S, ρ_g, P_{cloud}), the variances $v(K_c)$ and $v(K_{cb})$ are computed over the 20 values K_c and K_{cb}. Since the clouds and other atmospheric constituents are mixed up in the atmosphere, K_c, or K_{cb}, is expected to change with varying P_c. It is observed that $v(K_c)$ and $v(K_{cb})$ are very small with respect to the squared mean values of K_c

and K_{cb} for each triplet (θ_S, ρ_g, P_{cloud}), meaning that changes in K_c and K_{cb} with varying P_c are small, thus supporting Eq. 3.

In order to illustrate this and to present this vast amount of results in a synthetic manner, it is firstly observed that these quantities $v(K_c)$ and $v(K_{cb})$ do not vary in a noticeable way with the cloud geometry for a given triplet (θ_S, ρ_g, τ_c), i.e. that among the cloud properties for a given phase, the cloud optical depth τ_c is the most prominent one. As a consequence, it is possible to illustrate the findings by averaging $v(K_c)$ and $v(K_{cb})$ over the cloud geometry properties for each triplet (θ_S, ρ_g, τ_c). One obtains $mean(v(K_c))$ and $mean(v(K_{cb}))$. The positive root means of these averages are denoted $RM(v(K_c))$ and $RM(v(K_{cb}))$:

$$RM(v(K_c)) = \sqrt{mean(v(K_c))} \quad (4)$$

$$RM(v(K_{cb})) = \sqrt{mean(v(K_{cb}))}$$

$RM(v(K_c))$ gives at a glance the influence of P_c on K_c for all cloud geometries. A small $RM(v(K_c))$ means that the mean of $v(K_c)$ is small. The variance $v(K_c)$ and consequently $RM(v(K_c))$ are linked to $\partial K_c / \partial P_c$. The lower $RM(v(K_c))$, the lower the mean of $v(K_c)$, the lower the change in K_c with P_c, and finally the lower the error made when using Eq. 3. The same reasoning holds for $RM(v(K_{cb}))$. $RM(v(K_c))$, respectively $RM(v(K_{cb}))$, can be considered as a measure of the error made on K_c, or K_{cb}, when using Eq. 3. These quantities are also expressed relative to the mean K_c and K_{cb} for a given triplet, yielding relative values, noted $rRM(v(K_c))$ and $rRM(v(K_{cb}))$.

4 Influence of P_c on clear-sky indices

Relative quantities $rRM(v(K_c))$ and $rRM(v(K_{cb}))$ depend on G and B. A large $rRM(v(K_c))$ may not be important if G is very small. To better understand the results, Figure 1 displays the averages of G and D for θ_S=40° as a function of ρ_g and τ_c for water cloud. The beam irradiance B is not drawn as it does not depend on ρ_g; it decreases rapidly as τ_c increases and the diffuse irradiance D tends towards G as a consequence. As expected, Fig. 1 shows that D increases with ρ_g, and that both G and D decrease as τ_c increases.

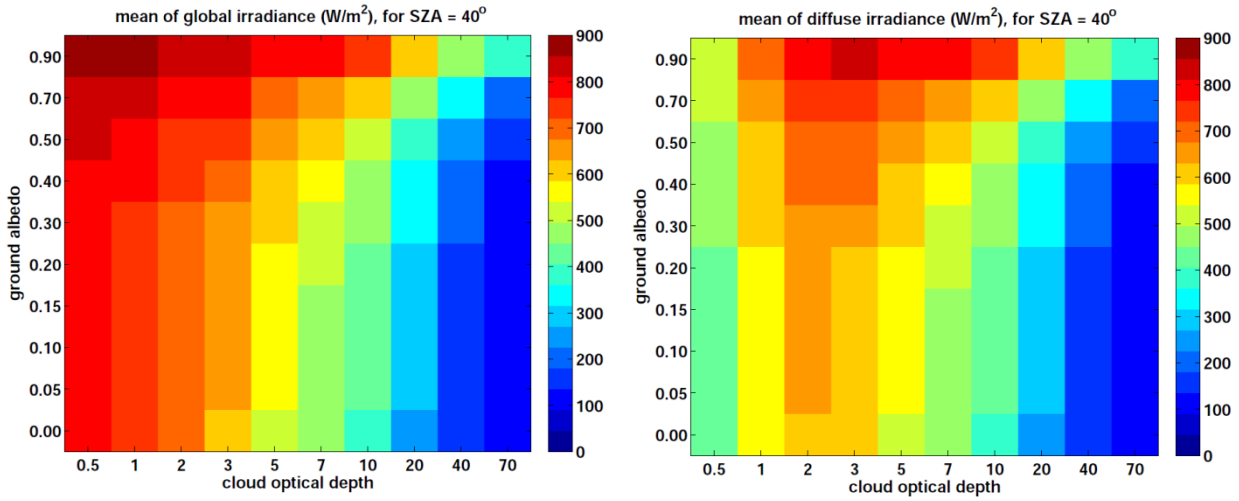

Figure 1. Average of G (left) and D (right) for θ_S=40° as a function of ρ_g and τ_c for water cloud.

Figure 2 exhibits $rRM(v(K_c))$ for each couple (ρ_g, τ_c) for θ_S=40° for water cloud (left) and ice cloud (right). Each cell represents the changes in K_c obtained for this θ_S and this couple (ρ_g, τ_c) when the geometrical parameters of the cloud and the other variables in P_c are varying. For both cloud phases, $rRM(v(K_c))$ increases with τ_c and ground albedo. As a whole, it is small. It is less than 2% for the most frequent cases, i.e. $\tau_c \leq 20$ and $\rho_g \leq 0.7$. It can be compared to the maximum relative errors (66 percent uncertainty) recommended by the World Meteorological Organization (WMO, 2008) for measurements of hourly means of G or D which are 2% for high quality, 8% for good quality, and 20% for moderate quality.

$rRM(v(K_c))$ reaches a maximum of 8.5% for τ_c=70 and ρ_g=0.9 for water cloud (7.5% for τ_c=20 for ice cloud). Large ρ_g and large τ_c mean more reflected radiation by the ground and more backscattered radiation by clouds. This increases the path of the radiation in the atmosphere, and therefore increases the influence of P_c on K_c. As G is small for (τ_c=70, ρ_g=0.9) (Fig. 1), a maximum of 8.5% is not important in absolute value since it corresponds to approximately 30 W m^{-2}. This high relative deviation happens only for very high ρ_g=0.9. When $\rho_g \leq 0.7$, the corresponding error on G is less than 10 W m^{-2}.

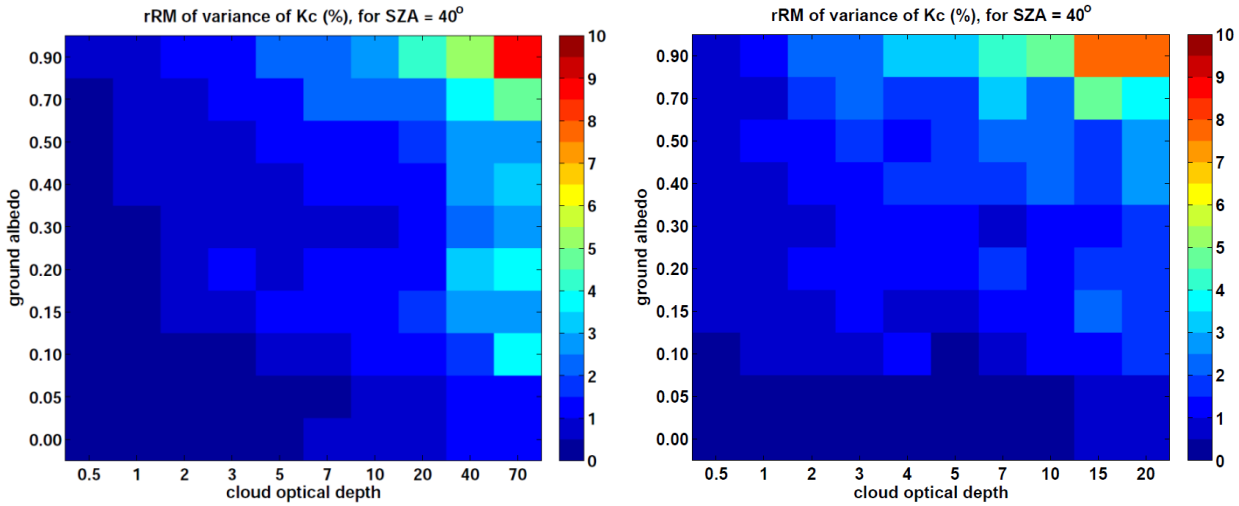

Figure 2. Relative root mean of variance of K_c due to changes in P_c as a function of ρ_g and τ_c for θ_S=40°, for water cloud (left) and ice cloud (right).

The median and percentiles 5% (P5) and 95% (P95) of $RM(v(K_c))$ for all corresponding couples (ρ_g, τ_c) for a given θ_S are computed and drawn in Fig. 3 for water cloud (left) and ice cloud (right) as a function of θ_S. They are also expressed relative to the corresponding mean K_c (Fig. 4) and are called relative median and relative P95. For both phases and for θ_S from 0° to 60°, the relative median is less than 2%, and the relative P95 ranges between 3.5% and 5%.

All three quantities increase sharply for θ_S>60°. The relative median, respectively P95, reaches a maximum of approximately 8-9%, respectively 11-12% for θ_S=80°. Then, a decrease is observed for θ_S>80°. Further computations show that the increase in relative influence with large θ_S is mostly due to the increase of the optical path in the atmosphere due to greater θ_S and therefore a greater influence of P_c and notably the aerosols.

Overall, an increase in τ_c or θ_S increases the path of the sun rays in the atmosphere, and therefore the influence of changes in P_c on K_c increases along with τ_c and θ_S. This increase is compensated by a corresponding decrease in G. Since G_c rarely reaches 120 W m^{-2} for θ_S=80°, the error in G corresponding to P95 is less than 15 W m^{-2}. The diffuse irradiance D and therefore G are strongly influenced by ρ_g. The influence of changes in P_c on K_c increases with ρ_g. Deserts such as Northern Africa and Arabia exhibit large ground albedo up to approximately 0.5 (Tsvetsinskaya et al., 2002; Wendler and Eaton, 1983); the error (P95) on

G is of order of 10 W m^{-2}. Fresh snow-covered or ice-covered areas may exhibit very large ρ_g. For ρ_g=0.9, the error on G can be large for small θ_S, i.e. 30 W m^{-2}. One has to be cautious in using Eq. 3 in such extreme cases.

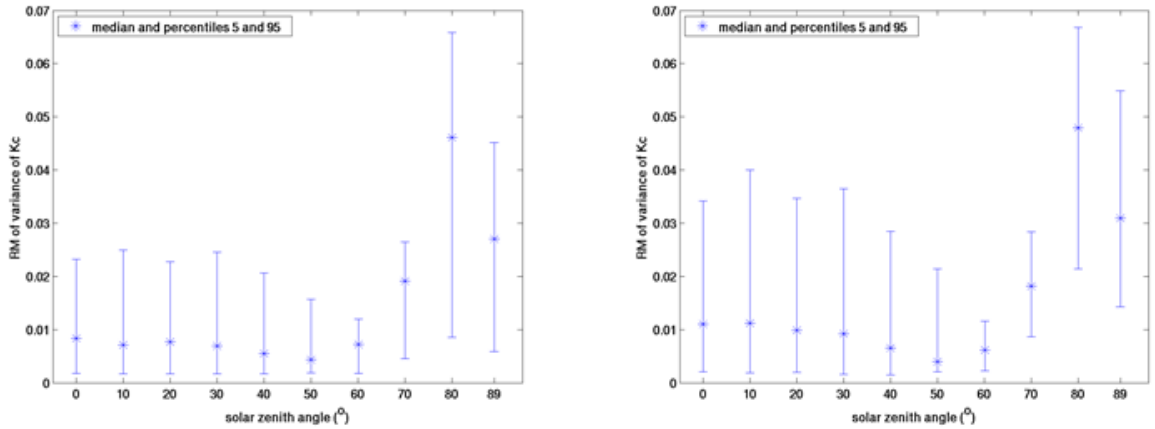

Figure 3. Median (star) and percentiles 5% and 95% of $RM(v(K_c))$ for all couples (ρ_g, τ_c) as a function of θ_S for water cloud (left) and ice cloud (right).

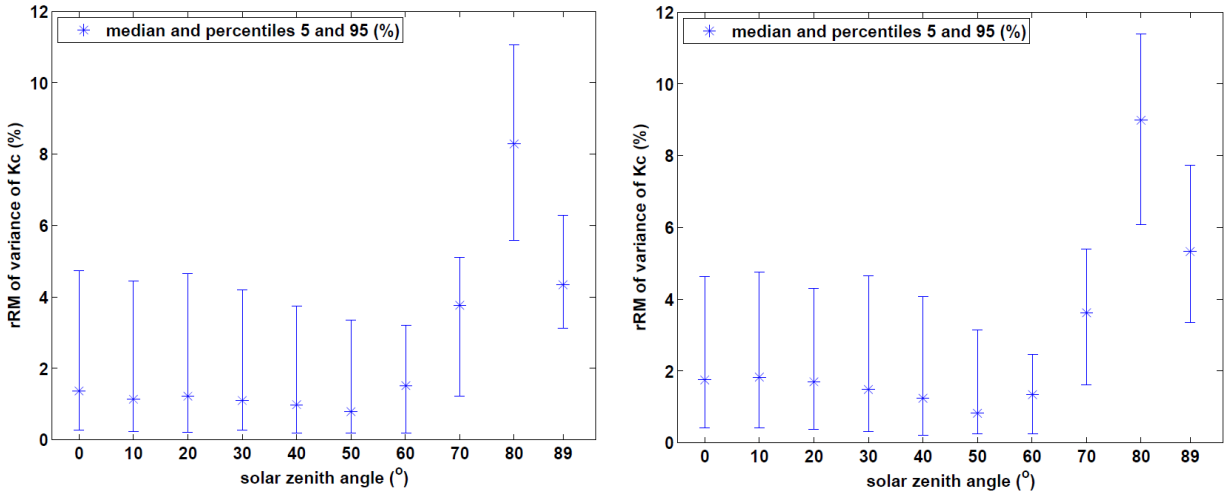

Figure 4. Median (star) and percentiles 5% and 95% of $RM(v(K_c))$ relative to the corresponding mean K_c for all couples (ρ_g, τ_c) as a function of θ_S for water cloud (left) and ice cloud (right).

Similar calculations are made for K_{cb}. As expected with a RTM code K_{cb} does not change with ground albedo nor cloud phase; the cloud optical depth is the most prominent variable. Fig. 5 exhibits the median and percentiles 5% and 95% of $RM(v(K_{cb}))$ for all couples (ρ_g, τ_c) as a function of θ_S and their value relative to the corresponding mean K_{cb}. The relative median, respectively relative P95, is less than 2%, respectively 3% for $\theta_S \leq 60°$. Then, it rises sharply. The relative median, respectively P95, reaches a maximum of approximately 8%, respectively 17% for $\theta_S=80°$. Then, a decrease is observed for $\theta_S>80°$. Large θ_S correspond actually to low irradiances. The clear-sky B_c equals 53 W m^{-2} for $\theta_S=80°$, and therefore the corresponding median and P95 errors in B are approximately 4 W m^{-2} and 9 W m^{-2}.

$rRM(v(K_{cb}))$ has a tendency to increase as θ_S increases. This increase is compensated by a corresponding decrease in B. The clear-sky irradiance B_c rarely reaches 90 W m^{-2} for $\theta_S=80°$ and the maximum error in B is less than 16 W m^{-2}.

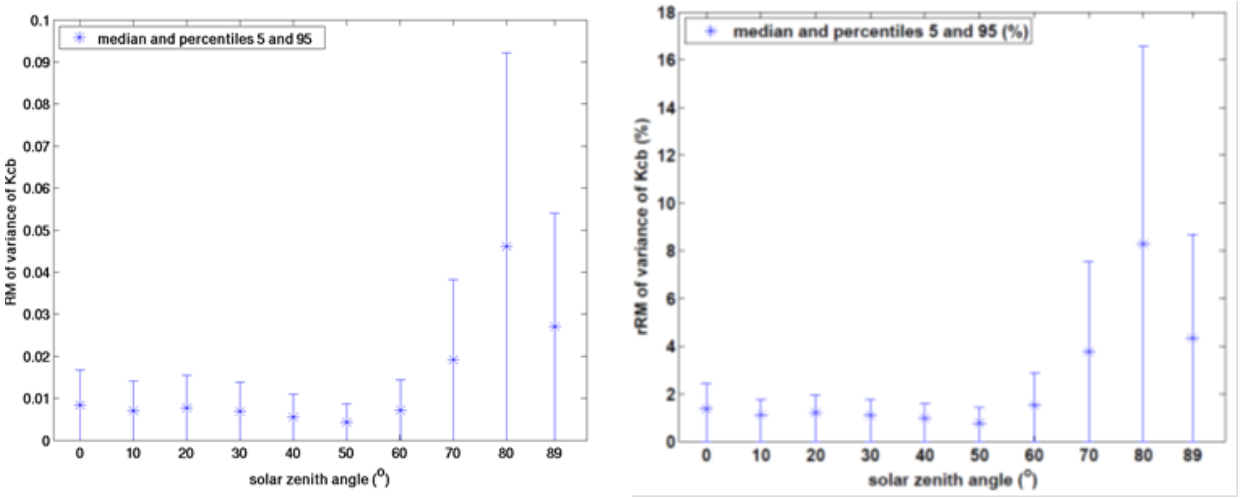

Figure 5. Median (star) and percentiles 5% and 95% of $RM(v(K_{cb}))$ for all couples (ρ_g, τ_c) as a function of θ_S. Absolute values (left), relative to the corresponding mean K_{cb} (right).

If cases of large θ_S and τ_c for which the radiation is greatly attenuated are removed by considering only cases for which G>100 W/m^2, the obtained $rRM(v(K_c))$ and $rRM(v(K_{cb}))$ are very small, even for large θ_S. For θ_S equal to 70° and 80°, the medians are approximately 3% of K_c and K_{cb}, and the P95 are 5% and 7% respectively.

It is concluded that for all considered cloud properties and θ_S, and for $\rho_g \leq 0.7$, the influence of changes in P_c on K_c and K_{cb} can be neglected. In these cases, Eq. 3 may be adopted with an error (P95) on G and B less than 15 W m^{-2} and most often less than 2-5% in relative value. These results match the WMO requirements for high quality measurements. However, in applications as discussed in the following section, there will be other sources of uncertainties, and the total uncertainty of any model using Eq. 3 will be greater and probably exceeding these WMO requirements.

A similar analysis has been made for two-layered clouds with ice cloud topping water cloud. The water and ice cloud properties have been taken from Table 3, where only water clouds with a height top less or equal to 5 km were considered since the minimum height of ice cloud base is 6 km. Accordingly, there were 5 (water cloud) * 3 (ice cloud) cases. Results and conclusions are similar to those for single-layered clouds.

5 Practical implications

A first practical interest in adopting Eq. 3 instead Eq. 2 is that two independent models -one for modelling G_c and B_c, the other for modelling the effects of clouds- can be used. If the approach selected to assess the SSI is based on a LUT-based model, using Eq. 3 means that two LUT-based models for K_c and K_{cb} can be computed with only one typical set P_{c0}, therefore strongly reducing the number of runs of the RTM. One may select the following P_{c0}:

- the middle latitude summer from the USA Air Force Geophysics Laboratory (AFGL) data sets is taken for the vertical profile of temperature, pressure, density, and volume mixing ratio for gases as a function of altitude,
- aerosol properties: optical depth at 550 nm is set to 0.20, Angström coefficient is set to 1.3, and type is continental average,
- total column content in water vapour is set to 35 kg m^{-2},
- total column content in ozone is set to 300 Dobson unit,
- elevation above sea level is 0 m.

It has been checked that the difference in K_c and K_{cb} using different typical sets P_{c0} was negligible providing the selected P_{c0} does not include extreme values.

As an example, this approach is that used in the MACC/MACC-II (Monitoring Atmosphere Composition and Climate) projects to develop the new Heliosat-4 method for a fast assessment of G, D and B (Qu, 2013; Qu et al., 2013). The McClear clear-sky model (Lefevre et al. 2013) is adopted in Heliosat-4 to compute G_c and B_c. The McClear abaci are very large since there are 10 dimensions. They concentrate most of the computational resources. It took approximately 6 months in computation time to compute all abaci. On the opposite, the abaci for K_c and K_{cb} have much less dimensions and much less nodes. Computation time was of order of a few hours only. If it were not possible to consider independently the clear-sky conditions and the cloudy conditions, the computation time for abaci combining the dimensions of McClear abaci and those for K_c and K_{cb} would have amounted to years. The immense gain in time justifies the slight loss in accuracy.

Except θ_S and ρ_g, inputs to both models are independent. This is another practical advantage of Eq. 3 since it allows to efficiently coping with the fact that P_c and P_{cloud} may not be available at the same spatial and temporal resolutions. This is exactly the case in the MACC/MACC-II projects. On the one hand, these projects are preparing the operational provision of global aerosol properties forecasts together with physically consistent total column content in water vapour and ozone (Kaiser et al., 2012; Peuch et al., 2009). These data are available every 3 h with a spatial resolution of approximately 100 km. They are inputs to the McClear model, yielding G_c and B_c. On the other hand, these projects are preparing the provision of P_{cloud} at high temporal (15 min) and spatial (3 km at nadir) resolutions from an appropriate processing of images taken by the Meteosat Second Generation satellites. P_{cloud} will be input to the K_c and K_{cb} models. Using Eq. 3 implies that the SSI may be computed at the best available time and space resolutions by resampling G_c and B_c, instead of resampling all variables contained in P_c.

6 Conclusion

This Technical Note analyses the influence of the prominent atmospheric parameters on the SSI, with the objective to find a practical way to speed up the calculations with a RTM. The

presented results have been obtained by the RTM libRadTran. It has been checked that the results and conclusions do not depend on this model by obtaining similar results with the Streamer RTM (Key and Schweiger, 1998).

It was found that for all considered cloud properties, solar zenith angles and ground albedos, the influence of changes in clear-atmosphere properties on K_c and K_{cb} is generally less than 2-5%, provided that the ground albedo is less than 0.7. This variation is similar to the typical uncertainty associated to the most accurate pyranometers. In these cases, Eq. 3 may be adopted with an error (P95) on G and B less than 15 W m^{-2}.

The longer the path of sun rays in the atmosphere, the greater this variation and the greater the influence of clear-atmosphere properties on the clear-sky indices. The mean error made when using Eq. 3 can reach significant relative values at high θ_S: 4% at 70° and 8% at 80°. However, in such cases, the irradiances are very low, and the error on global and direct irradiances expressed as the percentile 95% (P95) is less than 15 W m^{-2}. The P95 can be greater than 15 W m^{-2} when the ground albedo is greater than 0.7. In that case, one should be cautious in using Eq. 3. Such high albedos are rarely found, they may happen in case of fresh snow.

Like in other RTMs the beam irradiances are modelled by libRadtran as if the sun were a point source. On the contrary, pyrheliometers measure the radiation coming from the sun direction with a half-aperture angle equal to 2.5° according to WMO standards. The diffuse irradiance in this angular region is called the circumsolar irradiance (CSI). If it were to be compared to measurements, irradiances estimated in this work have to be corrected by adding CSI to B, and by removing CSI from D. In clear-sky, the CSI correction to B is approximately 1% of B (Gueymard 1995; Oumbe et al. 2012). Under cloudy skies, and especially thin clouds, the CSI can be greater than 50% of B. A CSI correction needs to be applied only in cloudy skies. Therefore the CSI can be taken into account *a posteriori* by correcting K_c and K_{cb} obtained by Eq. 4 with a specific model.

The presented work has demonstrated that computations of the SSI can be made by considering independently the clear-sky conditions and the cloudy conditions as shown in Eq. 3. A first practical interest is that two independent models may be developed and used, one for clear-sky conditions, and the other for cloudy conditions with their own set of inputs.

Another practical interest is that it allows to efficiently coping with cloud and clear-sky variables available at different spatial and temporal resolutions.

These results are important in the view of an operational system as it permits to separate the whole processing into two distinct and independent models, whose input variables types and resolutions may be different. The benefit of this separation is not limited to LUT-based models. For example, one may combine LUT-based models for K_c and K_{cb} with an analytical model predicting G_c and B_c such as the ESRA model (Rigollier, Bauer, and Wald, 2000) or the SOLIS model (Mueller et al., 2004). When both models are LUT-based, using Eq. 3 means two ensembles of abaci, one for clear-sky and the other for cloudy skies. In doing so, the number of entries for each ensemble is reduced leading to reducing *i)* the size of the abaci, *ii)* the number of combination between parameters, and *iii)* the total number of interpolations between nodes, thus increasing the speed in computation.

Acknowledgements

The research leading to these results has received funding from the European Union's Seventh Framework Programme (FP7/2007-2013) under Grant Agreement no. 218793 (MACC project) and no. 283576 (MACC-II project). MACC and MACC-II are preparatory projects for Europe's Global Monitoring for Environment and Security (GMES) program – recently re-named as the Copernicus programme. The authors thank the team developing libRadtran (http://www.libradtran.org). They also thank the anonymous reviewers whose efforts help in bringing clarity in our work.

References

Beyer, H.G., Costanzo, C., and Heinemann, D.: Modifications of the Heliosat procedure for irradiance estimates from satellite images, *Solar Energy*, 56, 207–212, doi: 10.1016/0038-092X(95)00092-6, 1996.

Blanc, P., Gschwind, B., Lefevre, M., and Wald, L.: The HelioClim project: Surface solar irradiance data for climate applications, *Remote Sens.*, 3, 343-361, doi:10.3390/rs3020343, 2011.

Calbo, J., Pages, D., and Gonzalez, J.-A.: Empirical studies of cloud effects on UV radiation: A review, *Review of Geophysics*, 43, RG2002, doi:10.1029/2004RG000155, 2005.

den Outer, P. N., H., Slaper, Kaurola, J., Lindfors, A., Kazantzidis, A., Bais, A. F. , Feister, U., Junk, J., Janouch, M., and Josefsson, W.: Reconstructing of erythemal ultraviolet radiation levels in Europe for the past 4 decades, *J. Geophys. Res. Atmos.*, 115, D10102, doi:10.1029/2009JD012827, 2010.

Deneke, H.M., Feijt, A.J., and Roebeling, R.A.: Estimating surface solar irradiance from Meteosat SEVIRI-derived cloud properties, *Remote Sens. Environ.*, 12, 3131-3141, doi: 10.1016/j.rse.2008.03.012, 2008.

Granier, C., Engelen, R., Simmons, A., and the MACC Management Team: An overview of the MACC European project. Geophysical Research Abstracts, 12, EGU2010-3112, EGU General Assembly 2010, held 2-7 May, 2010, Vienna, Austria, 2010.

Greuell, W., Meirink, J. F., and Wang, P.: Retrieval and validation of global, direct, and diffuse irradiance derived from SEVIRI satellite observations, *J. Geophys. Res. Atmos.*, 118, 2340–2361, doi:10.1002/jgrd.50194, 2013.

Gueymard, C.A.: SMARTS, A simple model of the atmospheric radiative transfer of sunshine: Algorithms and performance assessment. Technical Report No. FSEC-PF-270-95. Cocoa, FL: Florida Solar Energy Center, 1995.

Huang, G.H., Ma, M.G., Liang, S.L., Liu, S.M., and Li, X.: A LUT-based approach to estimate surface solar irradiance by combining MODIS and MTSAT data, *J. Geophys. Res.*–*Atmos.*, 116, D22201, doi: 10.1029/2011JD016120, 2011.

Kaiser, J.W., Peuch, V.-H., Benedetti, A., Boucher, O., Engelen, R.J., Holzer-Popp, T., Morcrette, J.-J., Wooster, M.J., and the MACC-II Management Board: The pre-operational GMES Atmospheric Service in MACC-II and its potential usage of Sentinel-3 observations, ESA Special Publication SP-708, Proceedings of the 3rd MERIS/(A)ATSR and OCLI-SLSTR (Sentinel-3) Preparatory Workshop, held in ESA-ESRIN, Frascati, Italy, 15-19 October 2012, 2012.

Key, J., and Schweiger, A.J.: Tools for atmospheric radiative transfer: Streamer and Flux Net, *Computers & Geosciences*, 24, 443-451, 1998.

Lefevre, M., Oumbe, A., Blanc, P., Espinar, B., Gschwind, B., Qu, Z., Wald, L., Schroedter-Homscheidt, M., Hoyer-Klick, C., Arola, A., Benedetti, A., Kaiser, J., W., and Morcrette, J.-J.: McClear: a new model estimating downwelling solar radiation at ground level in clear-sky conditions, *Atmos. Meas. Tech.*, 6, 2403–2418, doi: 10.5194/amt-6-2403-2013, 2013.

Liou, K.: On the absorption and reflection and transmission of solar radiation in cloudy atmospheres, *J. Atmos. Sci.*, 33, 798–805, doi: 10.1175/1520-0469(1976)033<0798:OTARAT>2.0.CO;2, 1976.

Mayer, B. and Kylling, A.: Technical note: The libRadtran software package for radiative transfer calculations - description and examples of use, *Atmos. Chem. Phys.*, 5, 1855-1877, doi:10.5194/acp-5-1855-2005, 2005.

Mueller, R., Dagestad, K.F., Ineichen, P., Schroedter, M., Cros, S., Dumortier, D., Kuhlemann, R., Olseth, J.A., Piernavieja, G., Reise, C., Wald, L., and Heinnemann, D.: Rethinking satellite based solar irradiance modelling - The SOLIS clear-sky module, *Remote Sens. Environ.*, 91, 160-174, doi:10.1016/j.rse.2004.02.009, 2004.

Mueller, R., Matsoukas, C., Gratzki, A., Behr, H., and Hollmann, R.: The CM-SAF operational scheme for the satellite based retrieval of solar surface irradiance - a LUT based eigenvector hybrid approach, *Remote Sens. Environ.*, 113, 1012–1024, doi:10.1016/j.rse.2009.01.012, 2009.

Oumbe, A.: Exploitation des nouvelles capacités d'observation de la terre pour évaluer le rayonnement solaire incident au sol (Assessment of solar surface radiation using new earth observation capabilities). PhD thesis, MINES ParisTech, 9 November 2009 (128 pages).

Oumbe, A., Blanc, Ph., Gschwind, B., Lefevre, M., Qu, Z., Schroedter-Homscheidt, M., and Wald, L.: Solar irradiance in clear atmosphere: study of parameterisations of change with altitude, *Adv. Sci. Res.*, 6, 199-203, doi:10.5194/asr-6-199-2011, 2011.

Oumbe A., Qu, Z., Blanc, P., Bru, H., Lefevre, M., and Wald, L.: Modeling circumsolar irradiance to adjust beam irradiances from radiative transfer models to measurements, EMS Annual Meeting 2012, 10-14 September 2012, Lodz, Poland, 2012.

Peuch, V.-H., Rouil, L., Tarrason, L., and Elbern, H.: Towards European-scale Air Quality operational services for GMES Atmosphere, 9th EMS Annual Meeting, EMS2009-511, 9th European Conference on Applications of Meteorology (ECAM) Abstracts, held 28 Sept. -2 Oct. 2009, Toulouse, France, 2009.

Qu, Z.: Modélisation du transfert radiatif en atmosphère nuageuse en vue de l'estimation du rayonnement solaire au sol (Modeling radiative transfer in cloudy atmosphere to assess surface solar irradiance), PhD Thesis, MINES ParisTech, Paris, France, 2013.

Qu, Z., Oumbe, A., Blanc, P., Espinar, B., Gschwind, B., Lefevre, M., Wald, L., Gesell, G., and Schroedter-Homscheidt, M.: Fast radiative transfer parameterisation for assessing the surface solar irradiance – the Heliosat-4 method, submitted to *Atmos. Meas. Tech.*, 2014.

Rigollier, C., Bauer, O., and Wald, L.: On the clear sky model of the 4th European Solar Radiation Atlas with respect to the Heliosat method, *Solar Energy*, 68, 33-48, doi: 10.1016/S0038-092X(99)00055-9, 2000.

Rossow, W., and Schiffer, R.: Advances in understanding clouds from ISCCP, *B. Am. Meteorol. Soc.*, 80: 2261-2287, doi:10.1175/1520-0477(1999)080<2261:AIUCFI>2.0.CO;2, 1999.

Schulz, J., Albert, P., Behr, H.-D., Caprion, D., Deneke, H., Dewitte, S., Dürr, B., Fuchs, P., Gratzki, A., Hechler, P., Hollmann, R., Johnston, S., Karlsson, K.-G., Manninen, T., Müller, R., Reuter, M., Riihelä, A., Roebeling, R., Selbach, N., Tetzlaff, A., Thomas, W., Werscheck, M., Wolters, E., and Zelenka, A.: Operational climate monitoring from space: the EUMETSAT Satellite Application Facility on Climate Monitoring (CM-SAF), *Atmos. Chem. Phys.*, 9, 1687-1709, doi:10.5194/acp-9-1687-2009, 2009.

Stamnes, K., Tsay, S.-C., Wiscombe, W., and Jayaweera, K.: Numerically stable algorithm for discrete–ordinate–method radiative transfer in multiple scattering and emitting layered media, *Appl. Opt.*, 27, 2502–2509, doi: 10.1364/AO.27.002502, 1988.

Tselioudis, G., Rossow, W. B., and Rind, D.: Global patterns of cloud optical thickness variation with temperature, *J. Climate*, 5, 1484–1495, doi:10.1175/1520-0442(1992)005<1484:GPOCOT>2.0.CO;2, 1992.

Tsvetsinskaya, E. A., Schaaf, C. B., Gao, F., Strahler, A. H., Dickinson, R. E., Zeng, X., and Lucht, W.: Relating MODIS-derived surface albedo to soils and rock types over Northern Africa and the Arabian peninsula, *Geophysical Research Letters*, 29(9), 1353, 10.1029/2001GL014096, 2002.

Wendler, G., and Eaton, F.: On the desertification of the Sahel zone, *Climatic Change*, 5, 365-380, 1983.

WMO: Guide to meteorological instruments and methods of observation, World Meteorological Organization, WMO no 8, 7th Edn, Geneva, Switzerland, 2008.